REPORT DOCUMENTATION PAGE

The public reporting burden for this collection of information is estimated to average 1 hour per response, including the time for reviewing instructions, searching existing data sources, gathering and maintaining the data needed, and completing and reviewing the collection of information. Send comments regarding this burden astimata or any other espect of this collection of information, including suggestions for reducing the burdan, to the Department of Defense, Executive Services and Communications Directorate (0704-0188). Respondents should be aware that notwithstanding any other provision of law, no person shall be subject to any penalty for failing to comply with a collection of information if it does not display e currently valid OMB control number.
PLEASE DO NOT RETURN YOUR FORM TO THE ABOVE ORGANIZATION.

1. REPORT DATE (DD-MM-YYYY)	2. REPORT TYPE		3. DATES COVERED (From - To)
17-07-2009	Journal Article		

4. TITLE AND SUBTITLE	5a. CONTRACT NUMBER
Subinertial Slope-Trapped Waves in the Northeastern Gulf of Mexico	
	5b. GRANT NUMBER
	5c. PROGRAM ELEMENT NUMBER
	0601153N

6. AUTHOR(S)	5d. PROJECT NUMBER
Z. R. Hallock, W. J. Teague and E. Jarosz	
	5e. TASK NUM8ER
	5f. WORK UNIT NUMBER
	73-8554-A7-5

7. PERFORMING ORGANIZATION NAME(S) AND ADDRESS(ES)	8. PERFORMING ORGANIZATION REPORT NUMBER
Naval Research Laboratory Oceanography Division Stennis Space Center, MS 39529-5004	NRL/JA/7320--07-8001

9. SPONSORING/MONITORING AGENCY NAME(S) AND ADDRESS(ES)	10. SPONSOR/MONITOR'S ACRONYM(S)
Office of Naval Research 800 N. Quincy St. Arlington, VA 22217-5660	ONR
	11. SPONSOR/MONITOR'S REPORT NUMBER(S)

12. DISTRIBUTION/AVAILABILITY STATEMENT

Approved for public release, distribution is unlimited.

13. SUPPLEMENTARY NOTES

14. ABSTRACT

Current velocity from moored arrays of acoustic Doppler current profilers (ADCPs) deployed on the outer shelf and slope, south of Mobile Bay in the northeastern Gulf of Mexico, shows evidence of alongslope, generally westward-propagating subinertial baroclinic Kelvin waves with periods of about 16 and 21 days, amplitudes of 5 -10 cm s^{-1}, and wavelengths of about 500 km. The observed waves were highly coherent over the slope between about 200 and 500 m and accounted for a significant amount of the current variability below 200 m. The source of the waves could be attributed to effects of the Loop Current on the west Florida slope but is more likely due to direct forcing by Loop Current -generated eddies impacting the experimental area.

15. SUBJECT TERMS

ADCP, subinertial waves, baroclinic

16. SECURITY CLASSIFICATION OF:			17. LIMITATION OF ABSTRACT	18. NUMBER OF PAGES	19a. NAME OF RESPONSIBLE PERSON
a. REPORT	b. ABSTRACT	c. THIS PAGE			William Teague
Unclassified	Unclassified	Unclassified	UL	11	19b. TELEPHONE NUMBER (Include area code) 228-688-4734

Subinertial Slope-Trapped Waves in the Northeastern Gulf of Mexico

Z. R. HALLOCK

Planning Systems Incorporated, Slidell, Louisiana

W. J. TEAGUE AND E. JAROSZ

Naval Research Laboratory, Stennis Space Center, Mississippi

ABSTRACT

Current velocity from moored arrays of acoustic Doppler current profilers (ADCPs) deployed on the outer shelf and slope, south of Mobile Bay in the northeastern Gulf of Mexico, shows evidence of alongslope, generally westward-propagating subinertial baroclinic Kelvin waves with periods of about 16 and 21 days, amplitudes of 5–10 cm s^{-1}, and wavelengths of about 500 km. The observed waves were highly coherent over the slope between about 200 and 500 m and accounted for a significant amount of the current variability below 200 m. The source of the waves could be attributed to effects of the Loop Current on the west Florida slope but is more likely due to direct forcing by Loop Current–generated eddies impacting the experimental area.

1. Introduction

From May 2004 to May 2005 deep-current measurements were conducted by the Naval Research Laboratory in the northeastern Gulf of Mexico (GOM) just west of the DeSoto Canyon, over the outer shelf and on the upper part of the slope. Coherent current fluctuations at periods of about 16 and 21 days were observed over much of the water column on the slope shallower than 1000 m. The shelf–slope region of the northeastern GOM is characterized by the broad west Florida shelf, which slopes gently to a depth of about 1000 m and then more steeply to the basin floor near 3000 m (Fig. 1a). The isobaths turn west southwestward near the DeSoto Canyon and converge through the region south of Mobile Bay, forming a moderately steep slope of about 30-km width between about 100 and 1500 m. Farther southwest, the isobaths diverge as they pass south of the mouth of the Mississippi River. The observed 2–3-week current fluctuations described here were propagating along the isobaths west southwestward on the upper slope and trapped near 400 m. Possible generation agents include low-frequency waves propagating from

Corresponding author address: W. J. Teague, Naval Research Laboratory, Stennis Space Center. MS 39529-5004.
E-mail: teague@nrlssc.navy.mil

the deep GOM or along the west Florida slope and more local forcing by mesoscale eddies.

A number of studies describe low-frequency variability in the GOM and its interaction with the topography. Oey and Lee (2002) describe modeled deep eddy kinetic energy (EKE) in the GOM. They show a small area of elevated EKE on the slope between about 1000 and 2000 m south of Mobile Bay. It is not clear if this deep energy can penetrate onto the upper part of the slope in this region; Oey and Lee (2002) state that their model cannot adequately resolve smaller scales on the steeper slopes, and their model did not extend to depths shallower than 1000 m. The slope has been found to present a barrier to low-frequency motions propagating from deeper water (Csanady and Shaw 1983; Shaw and Peng 1987). On the other hand, Ou and Beardsley (1980) discuss topographic waves on a steep continental slope using a numerical model. They find that waves propagating onto the slope may excite baroclinic modes and produce cross-slope change in amplitude and phase.

Codiga et al. (1999), using a laboratory model (rotating tank) with dynamical similarity to our observational area, describe slope-trapped baroclinic Kelvin waves that propagate along isobaths with shallower water to the right (for rotation consistent with the Northern Hemisphere). The waves were forced at a selected frequency
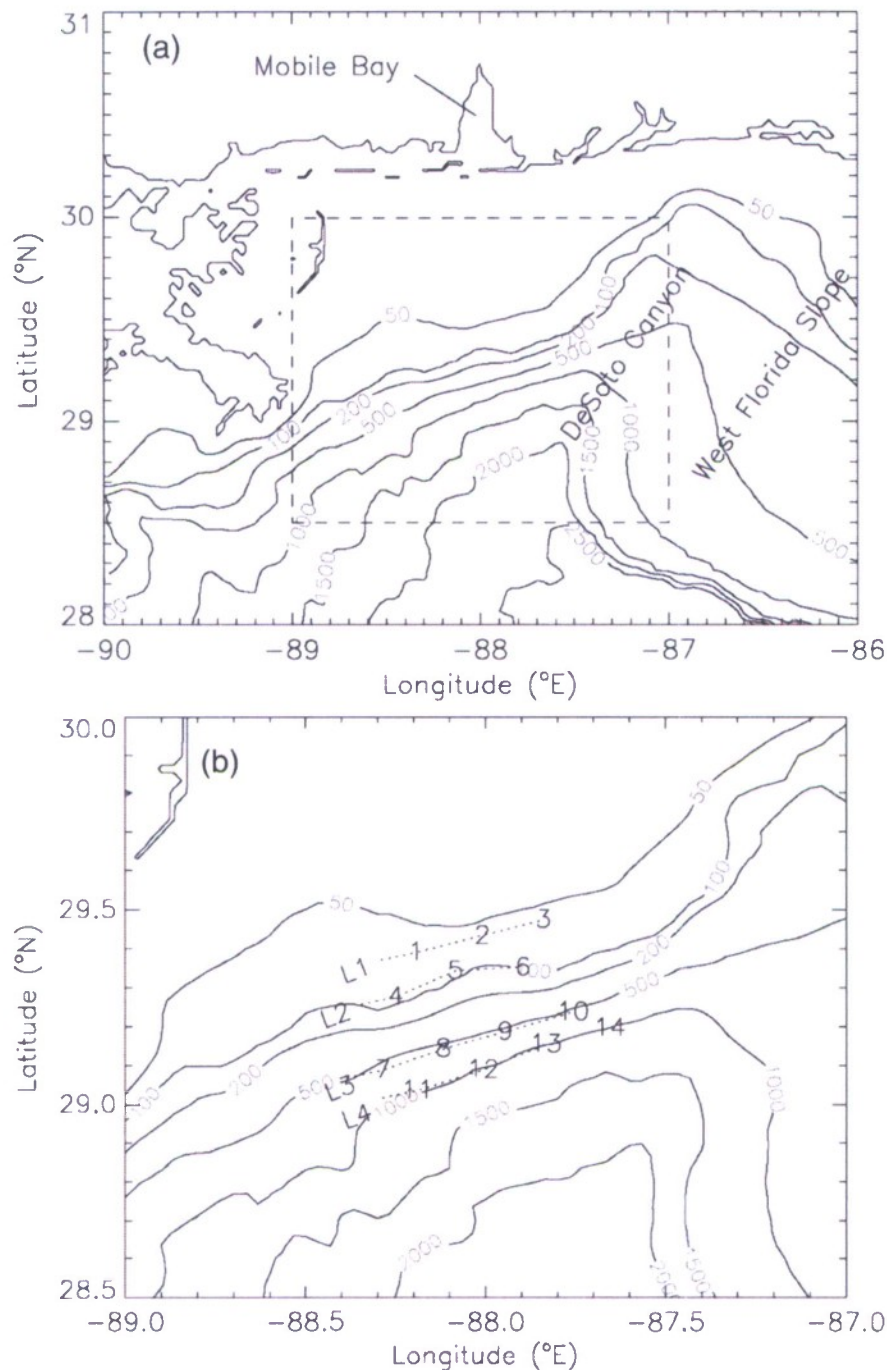
FIG. 1. Map of NE GOM: (a) overall setting. Box (dashed) indicates the observational area. (b) Expanded view: numerals indicate ADCP mooring locations; L1–L4 are the four approximately isobathic mooring lines.

by cross-isobath excitation. They found that these slope-Kelvin waves recovered their characteristics after encountering a canyon-like structure. Vangriesheim et al. (2005) describe slope-trapped biweekly subinertial waves off West Africa near 7°S; they interpret these observations as multiple modes of baroclinic coastal trapped waves. They discuss possible forcing by winds or the M_f tide, but suggest that these explanations are unlikely. Hetland et al. (1999) describe a jet along the edge of the west Florida shelf that was forced by the Loop Current (LC); such an event implies that the edge of the LC intruded onto the slope offshore of the shelf edge. The

location of the LC event was east and south of the DeSoto Canyon. The role of eddies interacting with slope topography in the NE GOM is described by Carnes et al. (2008), Hamilton and Lee (2005), and Wang et al. (2003). Hamilton and Lee (2005) found evidence of long-period (~100 day) downslope propagation associated with eddies. They also found variability in the 15–50-day band but did not see evidence of propagation. In this paper, we categorize and estimate space and time characteristics of the subinertial fluctuations and suggest a possible mechanism for their generation. Section 2 describes the observations. Section 3 describes analyses used and their results. Section 4 presents a discussion of the subinertial trapped waves. Section 5 provides a summary and conclusions.

2. Observations

Fourteen moorings were deployed in May 2004 for one year in the northeastern Gulf of Mexico just west of the DeSoto Canyon on the outer continental shelf and upper slope about 100 miles south of Mobile, Alabama (Fig. 1). The moorings were distributed along four lines with an average horizontal spacing between instruments of approximately 15 km. The water depths along the four lines (referred to as L1, L2, L3, and L4) were 60, 90, 500, and 1000 m, respectively. All 14 of the moorings were recovered in November 2004 and 13 were redeployed at the same locations. There is a gap of about a week between the deployments. The moorings were recovered in May 2005. Conductivity–temperature–and depth (CTD) profiles were also collected during each of the three cruises. The low-frequency currents for the first half of the deployment period are described by Teague et al. (2006) and for the second half of the deployment by Carnes et al. (2008). The moorings were affected by Hurricane Ivan in September 2004 (Teague et al. 2007). During and after the passage of Ivan, the slope currents were dominated by subinertial waves with a period of 2–5 days. Near-inertial motions were generated on the shelf and slope that lasted for about 10 days after the passage of Ivan.

All moorings contained acoustic Doppler current profilers (ADCPs). The six shelf moorings were deployed in trawl-resistant bottom mounts (TRBMs), called barnys because of their barnacle-like shape (Perkins et al. 2000), approximately along depth contours of 60 m (L1: M1–M3) and 90 m (L2: M4–M6). The barny moorings contained RD Instruments' Workhorse ADCPs operating at 300 kHz, Sea-Bird Electronics Model 26 wave–tide gauges, and EdgeTech acoustic releases for location and recovery. Nearly full water column velocity profiles were measured on the shelf every 15 min at 2-m

bin intervals. The eight slope moorings were deployed along the 500-m (L3: M7–M10) and 1000-m (L4: M11–M14) depth contours. They contained RD Instruments' Long Ranger ADCPs operating at 75 kHz mounted in flotation technology buoys, 45 in. in diameter. They measured velocity profiles every hour at 10-m bin intervals from about 50 m below the surface to about 500-m depth. The deep moorings along L4 were also equipped with Aanderaa RCM9 acoustic current meters that sampled every hour and were located about 100 m off the bottom at approximately 900-m depth. The random errors of the measured currents for the ADCPs, reported as a standard deviation, are about 1.30 cm s^{-1} for both the shelf and slope moorings. The random errors for the RCM9s are under 1 cm s^{-1}. More details on the moorings can be found in Teague et al. (2006) for the first half of the deployment and in Carnes et al. (2008) for the second half of the deployment. For the present work, the mooring data on the shelf were resampled at 1 h (after an appropriate low-pass filter was applied) to make them directly comparable to the slope moorings.

a. Bathymetry

The average orientation angle (γ) of the isobaths along the slope (Fig. 1) is about 20° counterclockwise (CCW) from east. The magnitude (α) of the downslope gradient is 0.0241 on the slope, based on a least squares fit of a plane to the areas bounded by latitudes 28.5°–29.5°N and longitudes 88.5°–87.5°W. The correlation between the bathymetry in this area with the fitted plane is 0.97. Local isobath orientations on the slope vary from about 14° to 33°, the larger value at M7. Isobath orientations for the shelf moorings (M1–M6) are not well defined since the magnitude of the depth gradient is considerably weaker than on the slope.

b. Velocity data

Samples of eastward (U) and northward (V) ADCP velocity time series at M8 (L3) at eight selected depths are shown in Fig. 2a. The velocities shown have been rotated 20° so that U is roughly parallel to the isobaths. Here, a bandpass filter (10–35d) was applied to emphasize the multiweek variability that is the focus of this study. Note the increase of 2–3-week fluctuation amplitude of velocity during the second half of the record and below about 200 m. Furthermore, these fluctuations are quite rectilinear (the more so near the bottom) and directed along-isobath. The other moorings on the slope (M7–M13) have similar characteristics. On the shelf the picture is different. Velocity time series for M6 (L2) are shown in Fig. 2b. Here, there is a slight increase in fluctuation amplitude in the latter part of
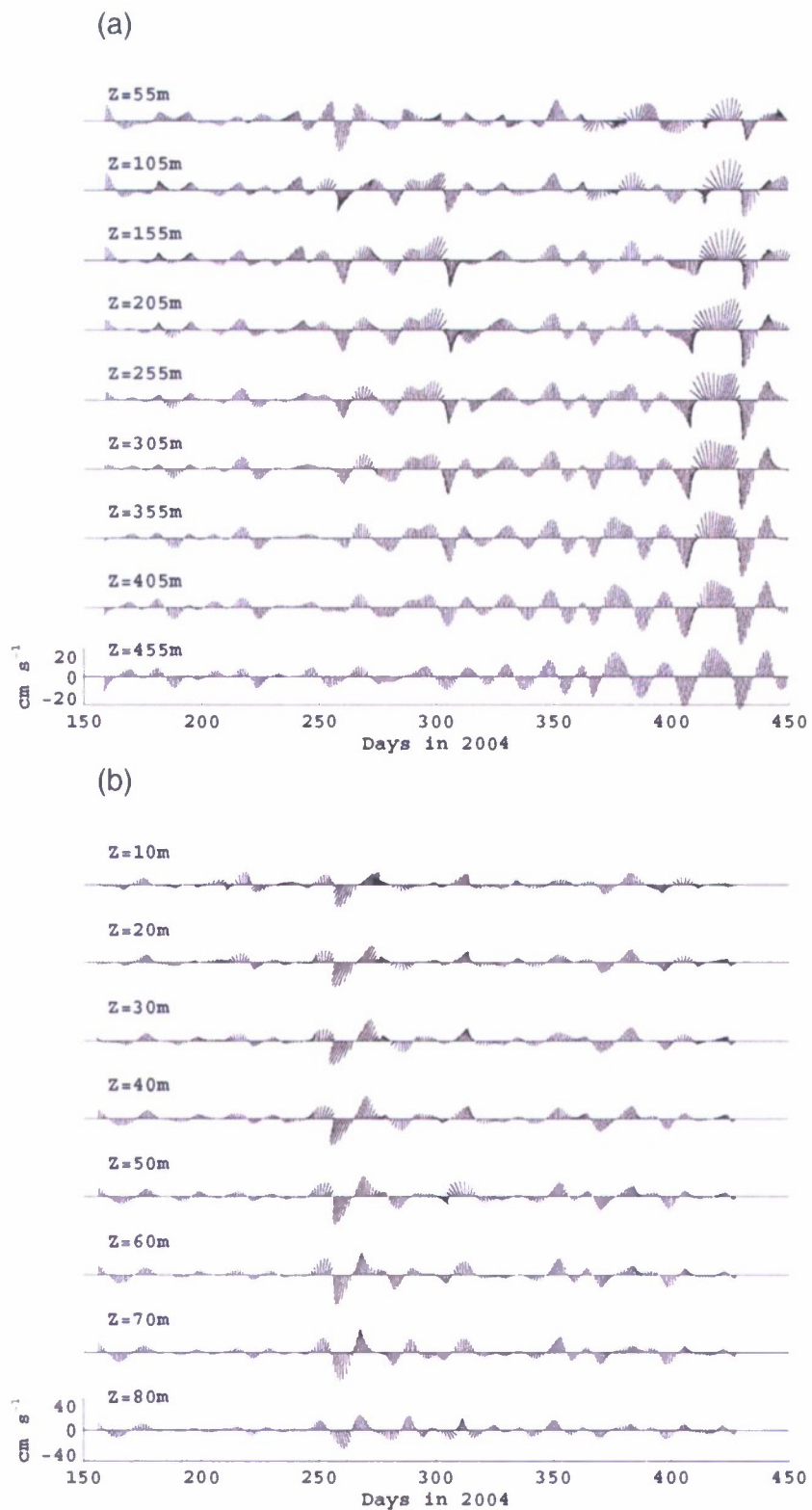
(a)

(b)

FIG. 2. Stick plots of bandpass-filtered current velocity from 35 to 10 days at selected depths. Vectors have been rotated so that upward is pointed 20° CCW from eastward (aligned roughly with the isobaths). (a) M8 and (b) M6.
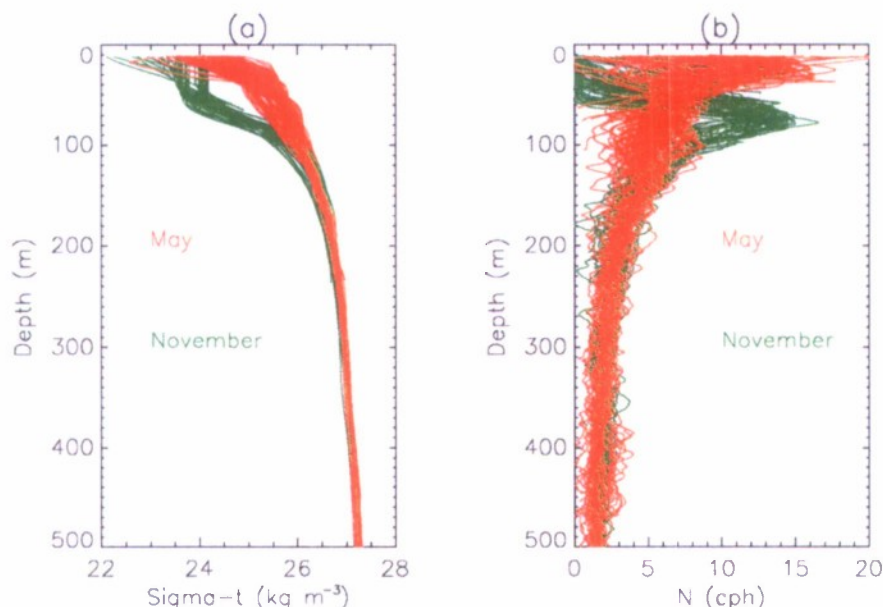
FIG. 3. (a) Density (σ_t) and (b) buoyancy frequency (N) from the deployment, turnaround, and recovery cruises: May (red) and November (green).

the record, but the vectors are not as rectilinear as for M8 and there is no particular change in amplitude with depth. There is a short-lived sharp increase in amplitude around day 260, which is the time that Hurricane Ivan passed over the moorings (Teague et al. 2007). As on the slope, the other shelf moorings generally exhibited similar characteristics. M1, however, showed more directional variability than the other moorings. Our analysis is focused on data from the second deployment, because it contains the longest uninterrupted records of the larger-amplitude 3-week fluctuations. Furthermore, M4 was not included in the analysis because the record is 26 days shorter than the other five shelf mooring records.

c. Stratification

Density (σ_t) and buoyancy frequency (N) profiles for most of the CTD casts collected during the cruises, conducted during May 2004, 2005, and November 2004, are plotted together in Figs. 3a,b. Above 300 m N ranges from about 1 to 20 cph. Below this depth, N converges to about 1.4 cph. The deeper parts of the profiles shown in Fig. 3 are typical of historical data south of the experimental area, well away from the slope, based on data from the World Ocean Database 1998 (WOD98) CD-ROM set (Conkright et al. 1998). In late fall (November), the main pycnocline was centered near 75 m; in late spring (May) it was shallower, generally less than 40 m. At and below the base of the pycnocline (~130 m), there was little seasonal change.

3. Spectral analysis of currents

a. Vertical dependence of spectra on the slope (L3)

The offshelf mooring records (M7–M13) from the second deployment appear to contain the strongest 3-week variability, and of these, the slope moorings L3, along the 500-m isobath (M7–M10), extend essentially over the whole water column. For maximum frequency resolution we use the entire (second deployment) record length as the fundamental period and average the corresponding four sample spectra of rotated U (at each depth), resulting in 8 degrees of freedom (DOF), or 4 equivalent degrees of freedom (EDOF). Variance-preserving auto spectra $[S_{uu}(z,f)]$ at three selected depths are plotted in Fig. 4a. Spectral peaks are evident in the upper water column at periods on the order of the record length (~175 days) and toward the bottom (350–450 m) at periods of 21.5 and 15.6 days. These latter peaks dominate the variance below about 300 m; shallower than this, other peaks (255 m) are comparable to the 15.6-day peak. Profiles of spectral energy (Fig. 4b) better show the depth dependence for the 21.5- and 15.6-day periods. The magnitude of the 21.5-day peak (near 415 m) is about 1.6 times that of the 15.6-day peak. The bandwidth associated with each harmonic is 0.00582 cpd, so the period bands represented by Fig. 5b are 20.2–22.9 and 14.9–16 days, respectively. Vertical coherence squared, relative to 415 m, and the associated phase for these two frequencies, appear in Figs. 4c and 4d. The 95% confidence level for squared coherence, for
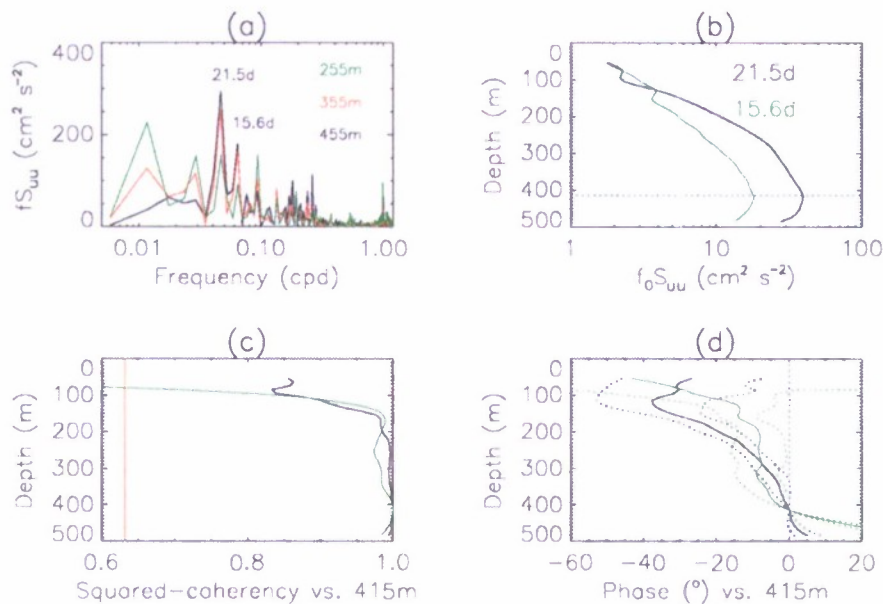
FIG. 4. Combined autospectra and cross-coherencies for alongslope currents from moorings on L3 (M7, M8, M9, M10). (a) Variance-preserving autospectra at three depths for frequencies between 0.01 and 1 cpd. (b) Spectral amplitude profiles for the 21.5-day (black) and 15.6-day (green) peaks; horizontal dotted line is at 415 m, and an ADCP bin is at the depth of the spectral maximum. (c) Vertical, squared coherency relative to 415 m for the same spectral peaks; vertical red line indicates minimum for significance at the 95% confidence level. (d) Vertical phase relative to 415 m; dotted profiles indicate errors for 95% confidence.

4 EDOF, is 0.63 (Emery and Thomson 2001; Thompson 1979) and is indicated by a vertical red line in Fig. 4c. The uncertainty in phase is indicated by the dashed curves in Fig. 4d. Clearly, fluctuations at these two frequencies are very coherent over the lower two-thirds of the water column. There is a significant increase of phase with increasing depth for the 21.5-day case; there is also a phase increase with depth for 15.6 days but it is of marginal significance. This phase difference indicates that deeper-current fluctuations lead those at shallower depths. The apparent upward propagation could be due to multiple dynamic modes at a single frequency; on the other hand, the presence of friction may introduce phase dependence within a single mode (e.g., Brink 2006). Figure 4b shows that energy at these two frequencies is mostly confined below the pycnocline (Fig. 3). There is also a slight falloff of energy below 415 m, possibly due to bottom boundary layer effects. Profiles with these amplitude and phase characteristics are similar to those predicted by Ou and Beardsley (1980) in their model of topographic waves on realistic slopes.

b. Combined vertical and horizontal cross-spectra

It is useful to examine auto- and cross-spectra for all 12 moorings (M1–M3, M5, M6, M7–M13) at the two periods (21.5 and 15.6 days) associated with the peaks in Fig. 4a. To gain confidence in spectral estimates for individual records, calculations were done using segments of 64.5 days in length, with a 50% overlap, yielding four segments over the record length and as before, 8 DOF (4 EDOF). This segment length was chosen to ensure that two of its harmonics (multiples of the fundamental frequency of 1/64.5 days) fall on or near the periods noted above. The third harmonic falls on a period of 21.5 days while the fourth falls on 16.1 days, different from the 15.6 days discussed above, but this difference is smaller than the spectral bandwidth. Each of the profiles was first subsampled in the vertical (for economy) to yield ten time series of velocity at each mooring position, or $U_{ij}(t)$, $V_{ij}(t)$, $i = 1, \ldots, 12; j = 1, \ldots, 10$. Subsampling in this way is reasonable because of the smooth vertical structure of the full-resolution spectral profiles of Fig. 4b. The subsampled dataset then consists of 120 series of U and of V, for a total of 240 time series. Velocities were rotated (as above) by 20°, and the 240 × 240 cross-spectral matrix (CS) of combined (U,V) data was computed. A compact way to evaluate CS is by calculating its eigenvalues and eigenfunctions (for each frequency of interest), in a frequency-domain empirical orthogonal function (FEOF) analysis (Wallace and Dickinson 1972). This technique identifies partitions or modes (not necessarily dynamical modes) maximizing coherence among the components (U_{ij}, V_{ij}). Then, for each frequency and each empirical mode we
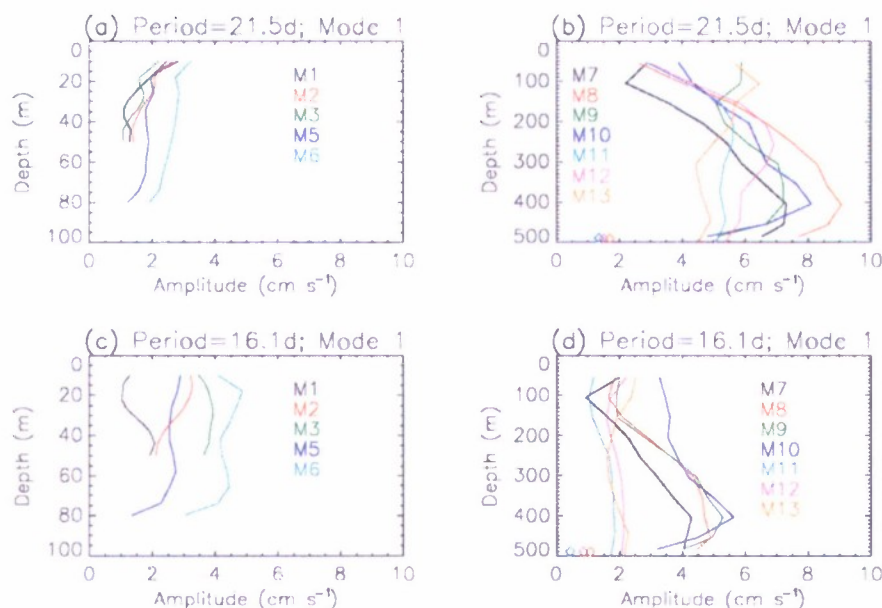
FIG. 5. Spectral amplitude profiles for mode 1 FEOFs for current velocities. Mooring location indicated by color: (left) M1–M6 and (right) M7–M13. Periods of (a),(b) 21.5 days and (c),(d) 16.1 days; (a),(c) shelf locations and (b),(d) slope locations; diamonds near lower abscissa axis are values for deep-current (~930 m) meters.

obtain spectral levels and current ellipse parameters at each mooring location and depth. In the indicated FEOF analysis, modes 1 and 2 explain 78% and 15% (for 21.5 days) and 62% and 28% (for 16.1 days) of total variance, respectively. Using the method of Overland and Preisendorfer (1982) we determined that only the first FEOF mode is significant for these two frequencies.

Mode 1 profiles of ellipse amplitude spectra are shown in Fig. 5. For the five shelf moorings (Fig. 5a), 21.5-day amplitudes are small and decrease slightly with increasing depth. For the seven slope moorings (Fig. 5b) the amplitudes are significantly greater and profiles for L3 (M7–M10) show a distinct maximum near 400 m. Amplitudes decrease upward from 400 m along L3; three of these decrease further above 150 m but the amplitudes at M9 and M13 increase above this depth. There was a strong event near the end of the record (the last month or so) that extends to these shallower depths that has likely leaked into the spectral estimates at these locations. A possible explanation is the impingement of an eddy at M13 and M9. Note that amplitudes decrease below 400 m for all slope moorings. Furthermore, for M11–M13, the amplitudes for the single current meter records (diamonds in Fig. 5) near 930 m are quite small. For the 16.1-day period (Fig. 5c), mode 1 amplitude profiles are similar in shape except for M1, which increases with depth to about twice its magnitude at 10 m. Amplitudes for the slope moorings (Fig. 5d) have shapes similar to those at the 21.5-day period but with

smaller magnitudes overall and a greater difference between L3 and L4 in the deeper regions. For both 21.5- and 16.1-day profiles, a downslope decrease in amplitude is evident between L3 and L4 near 400-m depth. The ratios of average amplitudes at L4–L3 (at these depths) is 0.67 and 0.41 for 21.5 and 16.1 days, respectively. The ratios of average amplitudes at L4 of the deep records near 930 m to those at L3 near 400 m are 0.19 and 0.15. The decrease in amplitude may indicate trapping along the slope for these fluctuations.

Mode 1 current ellipses for the periods discussed are plotted on maps of bathymetry (Figs. 6a,b) for depths: 44 m on L1, 74 m on L2, 405 m on L3, and 445 m on L4. These depths were chosen as representative of deep currents just above the bottom (L1–L2) and near deep maxima on L3. For L4, the ellipses are near 500 m, about half the water depth. Appearing just above each ellipse is its associated percent variance explained (PVE); this quantity is analogous to squared coherency for spectral estimates. At middepth on L3 (305 m; not shown), ellipses are broader (less eccentric) and slightly smaller in magnitude, and their orientations are a bit more variable about isobath orientations. Ellipse amplitudes and PVEs at 21.5 days (Fig. 6a) imply that most of the variability on the slope below the pycnocline is coherent, while at shallower depths and over the shelf there is significant uncorrelated energy. The smaller amplitudes on L4, relative to L3 (also noted in the previous paragraph), suggest trapping on the slope. The
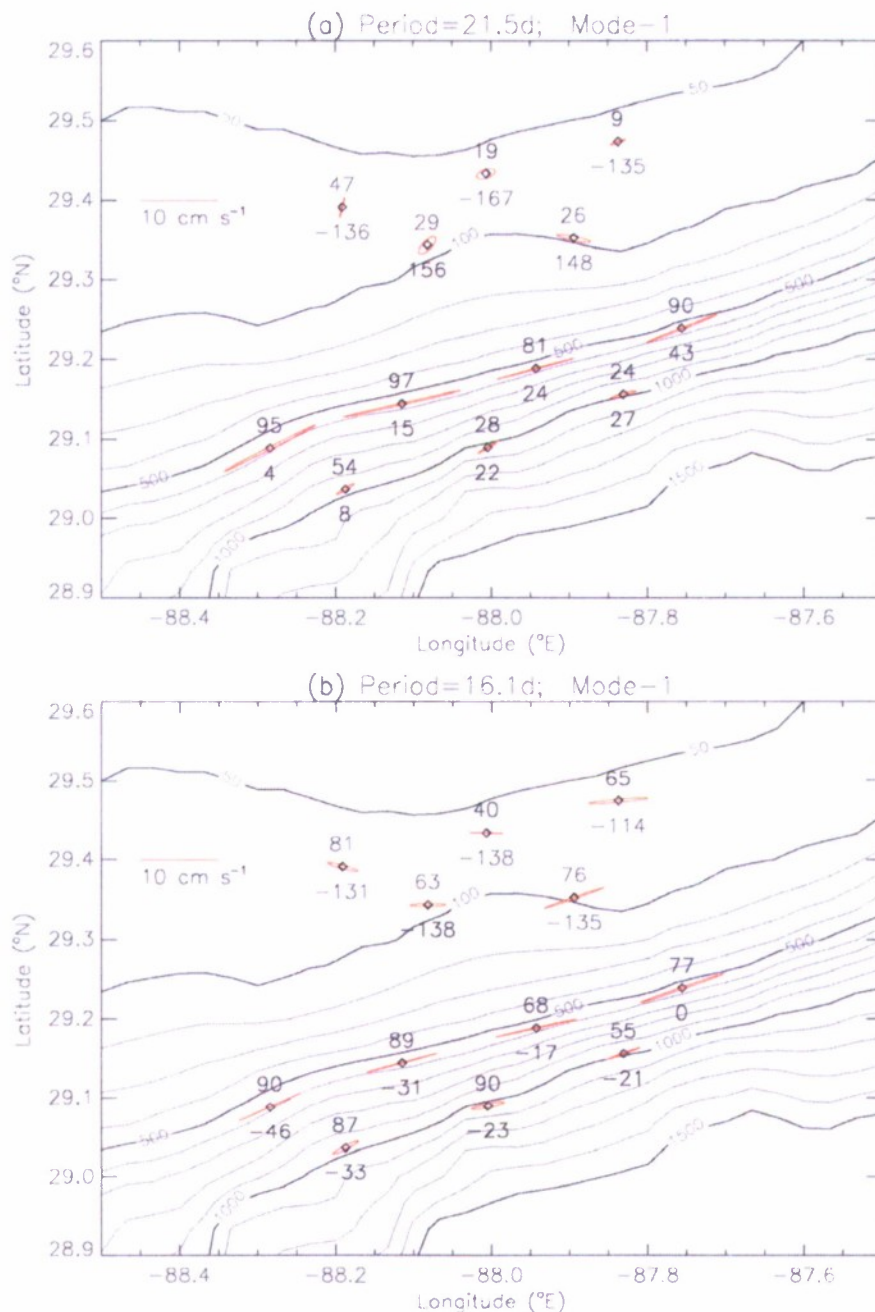
FIG. 6. FEOF mode 1 current ellipses for (a) 21.5 and (b) 16.1 days. Depths shown are 44 m on L1, 74 m on L2, 405 m on L3, and 445 m on L4. Numbers above (below) ellipses are percent variance explained (phase, deg).

sense of rotation of the current vector around the ellipses is positive (CCW) on L3, except at M9, and negative on L4. However, the ellipses are quite flat (especially on L3) and the sign may be ambiguous in light of uncertainties. At these depths (on L3) the minor axis of the ellipse for the average spectra of all four moorings (not shown) is essentially zero. Just below each ellipse is the temporal phase (°) of along-slope

velocity (U). Two points should be made about the phase differences. First, phases at the shelf locations (M1–M6) are nearly opposite (~150°) to those at the deep-slope locations (M7–M13); this phase reversal between deep and shallow locations might indicate a first baroclinic mode, coastal-trapped wave. Second, on the slope, phases generally increase eastward alongslope, suggesting westward propagation. It should be noted

that phases for the deep instruments (930 m) on M11–M13 show a similar change with alongslope distance (i.e., indicating westward propagation). For the 16.1-day fluctuations (Fig. 6b) we see smaller amplitudes over the slope and higher eccentricities for all ellipses. PVE values on L3, L4 are slightly lower, while those on L1, L2 are higher, showing similar content of correlated energy at all locations. As for 21.5 days, the 16.1-day ellipse orientations are closely aligned with isobaths at the slope locations. Phases show a similar horizontal trend over the slope but uncertainties are somewhat higher.

A progressive wave of the form $e^{i(kx-\sigma t)}$ is assumed where $\sigma = 2\pi/T$ is the angular frequency, T is the wave period, $k = 2\pi/\lambda$ is the wavenumber, and λ is wavelength. We estimate k with least squares fits of phase to alongslope distance for the records on L3: for 22.5 days, $k = 0.012 \pm 0.004$ km^{-1}, and for 16.1 days, $k = 0.015 \pm 0.007$ km^{-1}; errors are based on a confidence level of 90%. While the differences of wavenumbers for the two frequencies are within the error bounds, the least squares fits are excellent (correlations with alongslope distance are >0.99). A similar value of k is found on L4 for 21.5 days, with a larger error, but for 16.1 days the calculated k for L4 is smaller than the error. No significant trends of phase for the shelf locations are found, but the overall phase differences between shelf (L1, L2) and slope (L3, L4) are significant at 90% confidence. The wavenumber estimates for L3 imply wavelengths (λ) of 529 and 418 km, and wave phase speeds ($C_p = \sigma/k$) of 24.6 and 25.9 km day^{-1}, for periods of 21.5 and 16.1 days, respectively. We note that C_p values for both frequencies are nearly the same, suggesting a nondispersive wave.

4. Discussion

We conclude that the 21.5-day (and 16.1 day) fluctuations in our data, which are coherent over the slope over much of the water column, are likely to be a form of coastally trapped waves (CTWs), as defined in Wang and Mooers (1976). We first considered the possibility that the fluctuations were topographic Rossby waves (TRWs; Rhines 1970), similar to those found by Uehara and Miyake (2000) for biweekly current fluctuations over a similar bottom slope off the coast of Japan and by Hamilton (2007) for deeper regions of the GOM. However, with the wavelength range found here, the vertical trapping scale and relative steepness were found to be inconsistent with TRWs. We then considered a form of baroclinic Kelvin wave, as reported, for example, from observations in the Juan de Fuca Strait by Masson and Cummins (2000), who found a seaward-propagating internal Kelvin wave with a phase speed of about 50 km day^{-1}, and by Codiga et al. (1999, henceforth C99), who describe an internal Kelvin wave response to cross-slope forcing using laboratory simulations with a rotating tank. A simple baroclinic Kelvin wave is described (for alongslope velocity U) by

$$U \propto e^{(-y/R)} e^{i(kx-\sigma t)},\tag{1}$$

where y is the distance away from the vertical boundary (in this case downslope), $R = C_p/f$ is the baroclinic radius of deformation, f is the Coriolis parameter, and $C_p = \sigma/k = NH_1$ is the wave phase speed, which for Kelvin waves, does not depend on frequency (i.e., they are nondispersive); also, H_1 is the upper-layer depth for a two-layer baroclinic system and N is the buoyancy frequency in the pycnocline. From the FEOF results for the current velocity data we find $C_p = 25$ km day^{-1}, yielding $R = 4$ km. The average cross-slope distance between L3 and L4 is 8 km. For this estimated value of R, the decay of amplitude from L3 to L4 should be $e^{-8/4} = 0.13$, which is a greater falloff than that found from the data in the previous section—0.67 and 0.41 for 21.5 and 16.1 days, respectively, for the deepest ADCP bin on L4 (near 400 m, it is of the same order, however. On the other hand, the falloff found between L3 near 400 m and the deep-current meter records (930 m) was between 0.15 and 0.19, closer to the 0.13 found above; this result may be more germane since these records on both L3 and L4 were about the same distance from the bottom. As an independent check on these results, we look at hydrographic (CTD) measurements made during the experiment. From Fig. 3 we estimate these as 30 m and 10 cph, respectively, yielding $C_p = 45$ km day^{-1} and $R = 7$ km. The estimates are based on the spring (May) profiles, which are more likely to represent conditions during the portion of the record used in the analysis. These values are greater than those found from the velocity data, but are within a factor of 2. The uncertainties in the k values found above imply a range of C_p values of 19–37 km day^{-1} for 22.5 days and 18–48 km day^{-1} for 16.1 days, for a 90% confidence level; these come a bit closer to the value found from the CTD data.

C99, using laboratory simulations with a rotating tank, explored subinertial waves generated and trapped over a steep slope between a shelf and deep region. They compared their experiment to a typical coastal region having a shelf and slope profile very similar to that shown in Fig. 1. Their results showed flattened current ellipses over the slope deeper than the shelf break, oriented with major axes nearly parallel to the isobaths. Ellipse amplitudes showed relative maxima on

the lower part of the slope, decreasing offshore and upward. A relative minimum of amplitudes occurred just below the depth of the shelf break, above which they increased onshore and upward to another maximum near the bottom at the outer edge of the shelf. Above the minimum amplitude the ellipses broadened and their orientations rotated clockwise. Near the maxima over the shelf edge the ellipses were nearly circular. Temporal phases of the deep and shallow maxima differed by about π, indicating oppositely directed flow; such a configuration is consistent with a first-mode internal Kelvin wave. These results are similar to our findings (Fig. 6). In particular, nearly rectilinear, along-isobath current fluctuations are seen over the slope (L3, L4) below the depth of the shelf edge with broader ellipses and oppositely phased fluctuations just above the shelf edge (L2).

While C99 shows smaller but oppositely phased ellipses shallower than the shelf edge over the slope, our results show a phase change of about 40° between about 400 and 55 m. C99 had a constant value of buoyancy frequency N (comparable to our value below about 200 m) but did not contain a pycnocline, which, in our measurements (Fig. 3), occupied much of the water column over the shelf and reached the shallowest (55 m) bin in the L3 ADCPs. A different vertical modal structure might explain these differences.

It is not clear how the observed fluctuations were forced. Hamilton and Lee (2005) and Carnes et al. (2008) describe cyclonic and anticyclonic eddies, associated with Loop Current fluctuations, moving through the area of our observations (see, e.g., Fig. 15 in Carnes et al. 2008). Such eddies impacting the slope could excite CTWs as found by C99. Hamilton and Lee (2005) discuss low-frequency fluctuations on and near the slope resulting from eddy passage and find southward propagation for periods of about 100 days. They also find smaller-scale eddies with time scales on the order of 20 days near the DeSoto Canyon; they state that these eddies can cause strong cross-slope currents. Such currents might provide forcing analogous to that employed in the C99 experiments. However, for shorter periods of 15–50 days, Hamilton and Lee (2005) find low coherence and no significant phase differences over their array and hence no propagation; this result differs from ours in that we do find along-isobath propagation; this is perhaps due to a closer horizontal spacing of our arrays. Carnes et al. (2008), using daily Moderate Resolution Imaging Spectrometer (MODIS) images during winter 2005, detected eddies impacting the slope region of our observations. They found consistency with measured currents using the same dataset presented. Another interesting finding by C99 is that the slope-Kelvin waves

in their rotating tank model follow the topography, propagating along the slope, and are not drastically affected by the presence of a canyon projecting shoreward. This finding presents an alternative forcing scenario: the fluctuations evident in our observations may have propagated from off the west Florida slope and past the DeSoto Canyon, having been generated, perhaps, by the Loop Current or Loop Current–eddy interaction with the topography in that region, as suggested by Hetland et al. (1999).

Finally, the average alongslope velocities and associated standard deviations during winter and spring near 500-m depth were 4.2 and 11.1 cm s^{-1} for L3 and were 1.1 and 11.2 cm s^{-1} for L4 (see Table 2 of Carnes et al. 2008). The amplitudes of the internal Kelvin waves at periods of 21.5 days at depths below 400 m ranged from 4.5 to 9.0 cm s^{-1} (Fig. 5h). Since the amplitudes of the internal Kelvin waves are the same order of magnitude as the standard deviations of the observed currents near 500 m, much of the deep-current variability on the slope could be attributed to these waves.

5. Summary and conclusions

Evidence for baroclinic Kelvin waves with wavelengths of about 500 km and periods of 16 and 21.5 days was found along the upper slope in the northeastern Gulf of Mexico. Based on 170-day time series of current velocity from the outer shelf and slope south of Mobile Bay in the GOM, we found prominent spectral peaks for the along-isobath velocity component associated with the waves, primarily between 200 and 500 m on the slope. The current fluctuations at these periods were highly coherent at depth at all slope locations and partially coherent with shelf locations. Velocities on the slope were nearly rectilinear and aligned with isobaths. Currents related to the waves with maximum amplitudes of about 5 cm s^{-1} (16 day) and 9 cm s^{-1} (21.5 day) occurring between 400 and 500 m contributed significantly to the overall deep-current variability on the slope. Spatial structure in temporal phases (for 21.5 days) was consistent with west-southwestward, alongslope-propagating baroclinic Kelvin waves. Possible generation mechanisms include local forcing by smaller Loop Current–generated eddies at the head of the DeSoto Canyon or by Loop Current influence on the west Florida slope that then propagated past the DeSoto Canyon into the observational area.

REFERENCES

Brink, K. H., 2006: Coastal-trapped waves with finite bottom friction. *Dyn. Atmos. Oceans*, **41**, 172–190.

Carnes, M. R., W. J. Teague, and E. Jarosz, 2008: Low-frequency current variability observed at the shelfbreak in the northeastern Gulf of Mexico: November 2004–May 2005. *Cont. Shelf Res.*, **28**, 399–423.

Codiga, D. L., D. P. Renouard, and A. Fincham, 1999: Experiments on waves trapped over the continental slope and shelf in a continuously stratified rotating ocean, and their incidence on a canyon. *J. Mar. Res.*, **57**, 585–612.

Conkright, M. E., and Coauthors, 1998: World Ocean Database 1998: Documentation and quality control. National Oceanographic Data Center Internal Rep. 14, 114 pp.

Csanady, G. T., and P. T. Shaw, 1983: The insulating effect of a steep continental slope. *J. Geophys. Res.*, **88** (C12), 7519–7524.

Emery, W. J., and R. E. Thomson, 2001: *Data Analysis Methods in Physical Oceanography.* 2nd ed. Elsevier Science, 638 pp.

Hamilton, P., 2007: Deep-current variability near the Sigsbee Escarpment in the Gulf of Mexico. *J. Phys. Oceanogr.*, **37**, 708–726.

——, and T. N. Lee, 2005: *Eddies and Jets Over the Slope of the Northeast Gulf of Mexico, in Circulation in the Gulf of Mexico: Observations and Models, Geophys. Monogr.*, Vol. 161, Amer. Geophys. Union, 123–142.

Hetland, R. D., Y. Hsueh, R. R. Leben, and P. P. Niiler, 1999: A loop current–induced jet along the edge of the west Florida Shelf. *Geophys. Res. Lett.*, **26**, 2239–2242.

Masson, D., and D. F. Cummins, 2000: Fortnightly modulation of the estuarine circulation in Juan de Fuca Strait. *J. Mar. Res.*, **58**, 439–463.

Oey, L.-Y., and H.-C. Lee, 2002: Deep eddy energy and topographic Rossby waves in the Gulf of Mexico. *J. Phys. Oceanogr.*, **32**, 3499–3527.

Ou, H. W., and R. C. Beardsley, 1980: On the propagation of free topographic Rossby waves near continental margins. Part 2: Numerical model. *J. Phys. Oceanogr.*, **10**, 1323–1339.

Overland, J. E., and R. W. Preisendorfer, 1982: A significance test for principal components applied to a cyclone climatology. *Mon. Wea. Rev.*, **110**, 1–4.

Perkins, H., F. De Strobel, and L. Gauldesi, 2000: The Barny sentinel trawl-resistant ADCP bottom mount: Design, testing, and application. *IEEE J. Oceanic Eng.*, **25**, 430–436.

Rhines, P. B., 1970: Edge-, bottom- and Rossby waves in a rotating stratified fluid. *Geophys. Fluid Dyn.*, **1**, 273–302.

Shaw, P.-T., and C.-Y. Peng, 1987: A numerical study of the propagation of topographic Rossby waves. *J. Phys. Oceanogr.*, **17**, 358–366.

Teague, W. J., E. Jarosz, M. R. Carnes, D. A. Mitchell, and P. J. Hogan, 2006: Low-frequency current variability observed at the shelfbreak in the northeastern Gulf of Mexico: May–October, 2004. *Cont. Shelf Res.*, **26**, 2559–2582.

——, ——, D. W. Wang, and D. A. Mitchell, 2007: Observed oceanic response over the upper continental slope and outer shelf during Hurricane Ivan. *J. Phys. Oceanogr.*, **37**, 2181–2206.

Thompson, R. O. R. Y., 1979: Coherence significance levels. *J. Atmos. Sci.*, **36**, 2020–2021.

Uehara, K., and H. Miyake, 2000: Biweekly periodic deep flow variability on the slope inshore of the Kuril–Kamchatka Trench. *J. Phys. Oceanogr.*, **30**, 3249–3260.

Vangriesheim, A., A. M. Treguier, and A. Gael, 2005: Biweekly current oscillations on the continental slope of the Gulf of Guinea. *Deep-Sea Res. I*, **52**, 2168–2183.

Wallace, J. M., and R. E. Dickinson, 1972: Empirical orthogonal representation of time series in the frequency domain. Part I: Theoretical considerations. *J. Appl. Meteor.*, **11**, 887–892.

Wang, D.-P., and C. N. K. Mooers, 1976: Coastal-trapped waves in a continuously stratified ocean. *J. Phys. Oceanogr.*, **6**, 853–863.

——, L. Oey, T. Ezer, and P. Hamilton, 2003: Near-surface currents in DeSoto Canyon (1997–99): Comparison of current meters, satellite observation, and model simulation. *J. Phys. Oceanogr.*, **33**, 313–326.